Journal Pre-proof

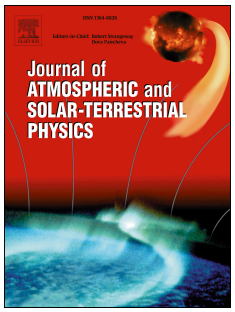

Determination of areas for surface refractivity variation analysis over Quebec

Yamina Bettouche, Basile Agba, Ammar Kouki, Huthaifa Obeidat, Haru Alhassan, Ali AlAbdullah, Jonathan Rodriguez, Raed Abd-Alhameed

PII: S1364-6826(20)30195-4

DOI: https://doi.org/10.1016/j.jastp.2020.105385

Reference: ATP 105385

To appear in: *Journal of Atmospheric and Solar-Terrestrial Physics*

Received Date: 5 November 2019

Revised Date: 7 July 2020

Accepted Date: 9 July 2020

Please cite this article as: Bettouche, Y., Agba, B., Kouki, A., Obeidat, H., Alhassan, H., AlAbdullah, A., Rodriguez, J., Abd-Alhameed, R., Determination of areas for surface refractivity variation analysis over Quebec, *Journal of Atmospheric and Solar-Terrestrial Physics* (2020), doi: https://doi.org/10.1016/j.jastp.2020.105385.

Determination of Areas for Surface Refractivity Variation Analysis Over Quebec

Yamina Bettouche[1], Basile Agba[1], Ammar Kouki[1], Huthaifa Obeidat[2*], Haru Alhassan[3], Ali AlAbdullah[3], Jonathan Rodriguez[4], Raed Abd-Alhameed[3]

[1]*École de Technologie Supérieure, Lacime, Montréal, Canada*
[2]*Faculty of Engineering, Jerash University, Jordan*
[3]*Faculty of Engineering and Informatics, University of Bradford, Bradford, UK*
[4]*Instituto de Telecomunicações, Campus Universitário de Santiago, Aveiro, Portugal*

Abstract

For the aim of surface refractivity analysis, the overall territory of Quebec has been divided in a desired number of areas from North to South using clustering analysis. The meteorological data used in the analysis are collected from 50 stations located in various climatic regions over Quebec for the year 2013. It is found that the best input data for the identification of areas is the water vapour pressure. The results show that the surface refractivity increase from North to South and the maximum values for all areas are observed in July or in August. However, the variation of the surface refractivity remains in a relatively small interval in comparison to the variation observed in some tropical countries, particularly Nigeria.

Keywords: Refractivity, Clustering Analysis, gradient refractivity.

1. INTRODUCTION

In the planning of terrestrial radio links, it is important to know the range of variations of the refractivity *N,* since it correlates highly with radio field strength. The paper analyzed the variation of the refractivity based on the data collected at the surface from 50 stations located

* Corresponding author
Email address: h.obeidat@jpu.edu.jo

at various climatic regions over Quebec. The study was motivated by the fact that Quebec has various climatic regions and in the same climatic region, there are mountainous as well as non- mountainous terrains, in other words, the surface refractivity depends not only of the meteorological parameters but also on the elevation in a given area. In these conditions, it is very important to divide the whole into various areas with pseudo similar of all (or at least some) parameters that determine *N*.

The radio refractivity measured in *N*-units (Freeman, 2006) (Guo and Li, 2000) depends on the meteorological parameters, particularly: temperature, humidity and partial water vapour pressure. Since these parameters vary with height *h* and season, the refractivity will also vary. Thus, in a given season, the refractivity will have a gradient *dN*/*dh*. Even small changes in the meteorological parameters may lead to a significant change of *N* and *dN*/*dh* (Priestley and Hill, 1985, Kablak, 2007, Ayantunji et al., 2011) (AbouAlmal et al., 2013). When such changes occur, they impact the radio link and may lead to reduced performance. For example, (Norland, 2006) reported the loss of radar coverage when important changes in the meteorological parameters occur while (Serdega and Ivanovs, 2007) reported a loss of microwave links with seasonal variations of *N*.

The knowledge of refractivity variation is important because this variation gives rise to the refraction of radio waves during their propagation through a stratified atmosphere. Such refraction can lead to a significant variation in received power level at the receiver (Ali et al., 2012) (Zilinskas et al., 2012). To obtain reliable communication links, several criteria, such as antenna heights and gains, power levels, path profile, distance, geographical location, atmospheric conditions and properties, etc., must be considered in the design/planning phase.

It is recommended to consider local meteorological parameters for a given geographical location since as noted in many published papers, the values provided by the ITU maps can be significantly different from the actual local data. For example, based on the data measured

locally, (Akpootu and Iliyasu, 2017) reported the variation of *N* over Ikeja city in Nigeria. The obtained results showed that the values of *N* in the rainy season are greater than those observed in the dry season. A paper published by (Kehinde, 2018) provides an analysis of *N* over Nigeria, the observed results showed that average yearly refractivity decreases with increase in latitude across Nigeria.

To the best of the author's knowledge, from reviewing the literature, there is no research dedicated to the analysis on the surface refractivity variation based on the meteorological data measured at stations located in various regions of Quebec. Such analysis is performed in this paper to identify the areas in Quebec from the north to the south with a similar variation of the surface refractivity.

The main contribution of this paper is to divide all territory of Quebec into the desired number of areas for surface refractivity variations analysis. These variations have to take into account both the seasonal variation of the meteorological parameters as well as the various altitudes across the territory. This is achieved by using clustering analysis (Dubes and Jain, 1988) (Kaufman and Rousseeuw, 2009). The clustering analysis allows grouping of objects (stations in this case) into several groups (areas) based on some input data which reflect the proximity between objects.

The rest of the paper is organized as follows. Section 2 provides the description of the data used and the theoretical background for the calculation of the radio refractivity, where the formulas used to estimate the surface refractivity are described. Section 3 describes the proposed algorithm to identify the areas. In Section 4, the obtained results are analyzed, and recommendations are given based on the analysis. And Finally, Section 5 highlights the summarized conclusions.

2. DATA USED AND CALCULATION OF RADIO REFRACTIVITY

In this paper, meteorological data (such as pressure, temperature, and relative humidity) measured at the surface from 50 stations are used to calculate the radio refractivity. These stations are listed in Table 1. The corresponding data can be found in the link provided of the acknowledgements section. For further analysis of using these data, we convert this data record to Excel files. It should also be noted that the analyzed year runs from December 2012 to November 2013.

The radio refractivity is an important parameter in the design of radio links. It depends essentially on the pressure *P*, temperature *T* and water vapour pressure *e*. This section describes the methodology used in this paper to estimate the surface refractivity from the measured *P*, *T* and *e*.

In the radio links analysis, the troposphere is viewed as a dielectric medium. Its refractive index, denoted by *n* is determined by (Sizun and de Fornel, 2005):

$$n = \sqrt{\varepsilon_r \mu_r} \qquad (1)$$

where ε_r is the relative permittivity and μ_r is the relative permeability. The index *n* has a mean value around 1.0003. Variations of *n* at ground level are in the range of $\pm 10^{-5}$ which is considered to be very low; however, these small variations cause radio waves to bend significantly over paths of several kilometres and have to be taken into account. For this reason, another index called refractivity and denoted here by *N* is used instead of *n*. These two indices are related by the following relationship (Sizun and de Fornel, 2005, Recommendation, 2001):

$$n = 1 + N \times 10^{-6} \qquad (2)$$

Equation 3 is used to determine the refractivity at the surface N_s (ITU, 2017):

$$N_s = 77.6\frac{P}{T} - 5.6\frac{e}{T} + 10^5\frac{e}{T^2} \quad (3)$$

where P and e are in hPa (hectopascal), and T is in K (Kelvin). The water vapour pressure is determined according to the following equation (Recommendation, 1999) (ITU, 2017):

$$e = \frac{He_s}{100} \quad (4)$$

where H is the relative humidity (%), and e_s (hPa) is the saturation vapour pressure determined by:

$$e_s = EF \cdot a \cdot e^{\left(\frac{bt - \frac{t^2}{d}}{t+c}\right)} \quad (5)$$

where

$$EF = 1 + 10^{-4}\left(7.2 + P(0.032 + 5.9 \times 10^{-6}t^2)\right) \quad (6)$$

And t is the temperature in ^{o}C a=6.1121, b=18.678, c=257.14 and d=234.5

3. ALGORITHM FOR AREAS IDENTIFICATION

The proposed algorithm to divide the stations into several areas is mainly based on using agglomerative hierarchical cluster analysis. Areas formed with only one, two or three stations are discarded by adding their stations in areas with more stations based on their latitude values. The flowchart of the proposed algorithm is shown in Figure 1

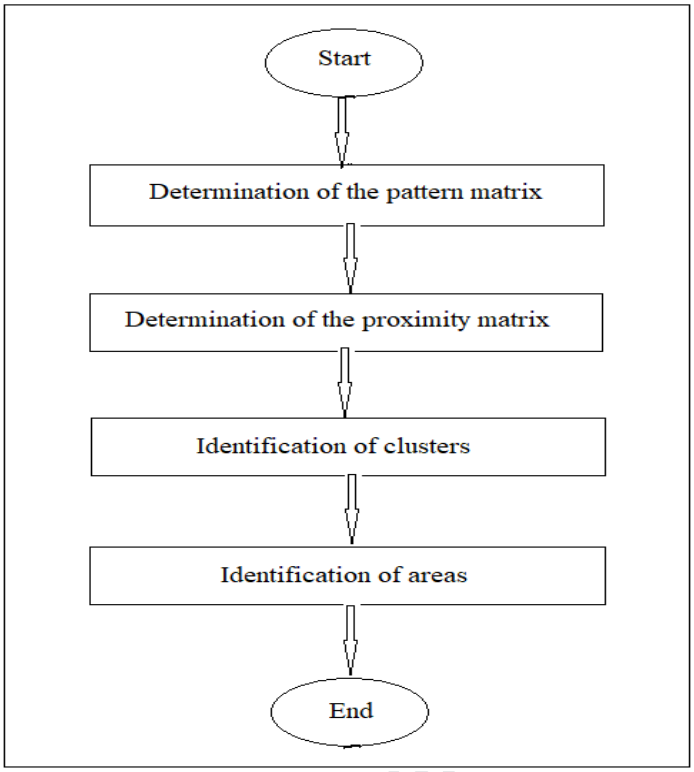

Figure 1: The Proposed algorithm for area's identification

As seen Figure 1, the algorithm consists of several steps. These steps are detailed below. Various functions from (Mathworks, 2013) are used to implement the proposed algorithm.

1) **Determination of the pattern matrix**. The pattern matrix (PM) contents the input data which reflect the proximity between the stations. Therefore, the choice or determination of the PM is very important. In this case, after some tries, we found that the parameter that allows forming the coherent areas is the water vapour pressure *e*. Therefore, PM has initially 50 rows (number of stations). Each row of the PM consists of the 12 mean monthly values of *e* for a given station. Note that It is necessary to normalize the PM before applying clustering analysis. There are many ways to normalize the data. In this paper, the normalized pattern matrix (NPM) is obtained from PM according to the following principle. Each entry x_{ij} of the PM is replaced by its normalized value according to:

$$x_{ij}^{n} = \frac{x_{ij} - \mu_i}{\sigma_i} \qquad (7)$$

where $\mu_i = \frac{1}{m}\sum_{j=1}^{m} x_{ij}$ and $\sigma_i = \frac{1}{m}\sqrt{\sum_{j=1}^{m}\left(x_{ij} - \mu_i\right)^2}$ are the mean and standard deviation of the i^{th} row of the PM respectively.

In our case, The PM has been normalized using the Matlab function '*zscore'*.

2) **Determination of the proximity matrix**. The distances between stations are calculated based on NPM. These distances are used to yield the proximity matrix *PMX*. The proximity matrix element PMX_{ij} between the stations *i* and *j* are determined by (Dubes and Jain, 1988), (Kaufman and Rousseeuw, 2009):

$$PMX_{ij} = \left(\sum_{k=1}^{N} \left|x_{ik}^{n} - x_{jk}^{n}\right|^{r}\right)^{1/r} \qquad (8)$$

where *r* is a fixed parameter; *N* is the number of stations; x_{ik}^{n} and x_{jk}^{n} are the entries of the NPM. The matrix *PMX* is obtained in our case with the Matlab function '*pdist'*.

3) **Identification of clusters**. A cluster consists of the closest stations that are linked at a given level. At the lowest level, all clusters have two stations. Note that at this level if the number of stations is odd there will be one cluster with only one station. If the number of obtained clusters is greater than two a matrix of distances between these clusters is calculated and then a larger cluster is formed by linking two closest clusters. This process will continue until the number of obtained clusters will be equal to two. The identification of clusters is done with the Matlab function '*linkage'*. The output of the function '*linkage'* is a hierarchical cluster tree, Z.

4) **Identification of areas**. Based on Z the Matlab function '*cluster'* is used to obtain the desired number of clusters. We retain only 5 largest clusters to form the desired areas. Each station which is in a cluster consisting of only one, two or three stations is added to a given one area according to the interval of latitudes the latitude of this station belongs.

4. RESULTS AND ANALYSIS

The proposed algorithm has been implemented in Matlab. This section gives the analysis of the obtained results. For simplicity of the analysis, the current section of the paper consists of 3 sub-sections: 1) Obtained areas, 2) Analysis of the yearly variations of N_s in various areas, and 3) Analysis of the monthly variations of N_s in various areas.

4.1 Obtained Areas

The meteorological data, used in this paper are collected from 50 stations located in various climatic regions over Quebec. Table 1 gives the names of these stations along with their corresponding geographical coordinates.

Table 1: List of stations geographic information

N^o	**Station**	**Latitude, ^{o}**	**Longitude, ^{o}**	**Altitude, m**
1	Ivujivik	62.42	-77.93	47.00
2	Parc Pingualuiyt	61.31	-73.67	503.40
3	Puvirnituq	60.05	-77.28	25.30
4	Aupaluq	59.30	-69.60	36.90
5	Kangiqsualujjuaq	58.71	-65.99	66.10

6	Kuujjuaq	58.10	-68.42	39.90
7	Kuujjuarapik	55.28	-77.75	12.20
8	Grande riviere	53.63	-77.70	194.80
9	Lac Eon	51.87	-63.28	588,90
10	Nemiscau	51.70	-76.12	244.50
11	Lac Benoit	51.53	-71.11	549.00
12	Lourdes de blanc	51.45	-57.18	37.20
13	Bonnard 1	50.73	-71.01	498.00
14	Havre St-Pierre	50.28	-63.61	37.80
15	Longue pointe	50.27	-64.23	11.00
16	Natashquan	50.19	-61.79	11.90
17	Port-Menier	49.84	-64.29	55.20
18	Chibougamau	49.77	-74.53	387.10
19	Matagami	49.76	-77.79	281.00
20	Pointe des monts	49.32	-67.38	5.90
21	Baie-Comeau	49.26	-68.15	129.50
22	Cap-Madeleine	49.25	-65.32	29.00
23	Cap-Chat	49.11	-66.65	5.00
24	Onatchiway	48.89	-71.03	304.00
25	Normandin	48.84	-72.55	137.20
26	Gaspe A	48.78	-64.48	34.10
27	Pointe au Pere	48.51	-68.47	4.90
28	Jonquiere	48.43	-71.14	135.60
29	Cap D’espoir	48.42	-64.32	15.40

30	Bagotville A	48.33	-71.00	159.10
31	Laterriere	48.31	-71.13	162.70
32	La Baie	48.30	-70.92	151.60
33	New Carlisle 1	48.01	-65.33	46.40
34	Parent	47.92	-74.62	444.70
35	L'étape	47.56	-71.23	791.20
36	La Tuque	47.41	-72.79	168.90
37	La Pocatiere	47.36	-70.03	31.00
38	Foret Montmorency	47.32	-71.15	672.80
39	Cap-Tourmente	47.08	-70.78	6.00
40	Lemieux	46.30	-72.06	97.20
41	Maniwaki AirPort	46.27	-75.99	199.70
42	Nicolet	46.23	-72.66	8.00
43	Beauceville	46.21	-70.97	229.20
44	L'assomption	45.81	-73.43	21.00
45	Montreal/St-Hubert	45.52	-73.42	27.40
46	Ottawa Gatineau	45.52	-75.56	64.30
47	Mctavish	45.51	-73.58	72.60
48	Montreal/P. E. Trudeau	45.47	-73.74	32.10
49	Sherbroke	45.44	-71.69	241.40
50	Granby	45.37	-72.77	86.00

Table 2 shows the obtained areas with their corresponding stations when N_{min} = 2 and N_{max} = 12. Note that in Table 2 for the sake of simplicity the stations are identified by their number according to the first column of Table 1.

Table 2: Identified areas with their stations

Area	Stations
1	1 to 6
2	7 to 11
3	12 to 23
4	24 to 36
5	37 o 50

4.2 Analysis of yearly variations of Ns in various Areas

The mean yearly variations of N_s in the five identified areas are shown in Figure 2.

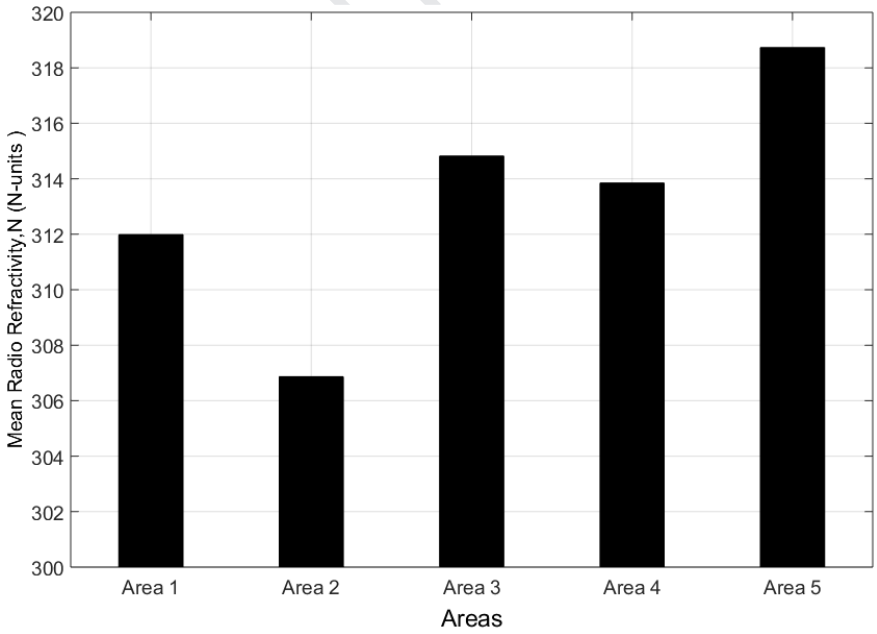

Figure 2: Mean yearly variations of *N* by area

From Figure 2 the mean yearly value of N_s increases from north to south for area 1, area 3 and area 5. The other way around is observed for area 2 and area 4. This is because in these areas, the stations have relatively high values of altitude. If the altitude is high, the value of

atmospheric pressure will decrease, and this will lead to a decrease of N_s. To illustrate this phenomenon, since the pressure P is the parameter that contributes above 70% of the value of N_s, Figure 3 shows the yearly mean values of P by area.

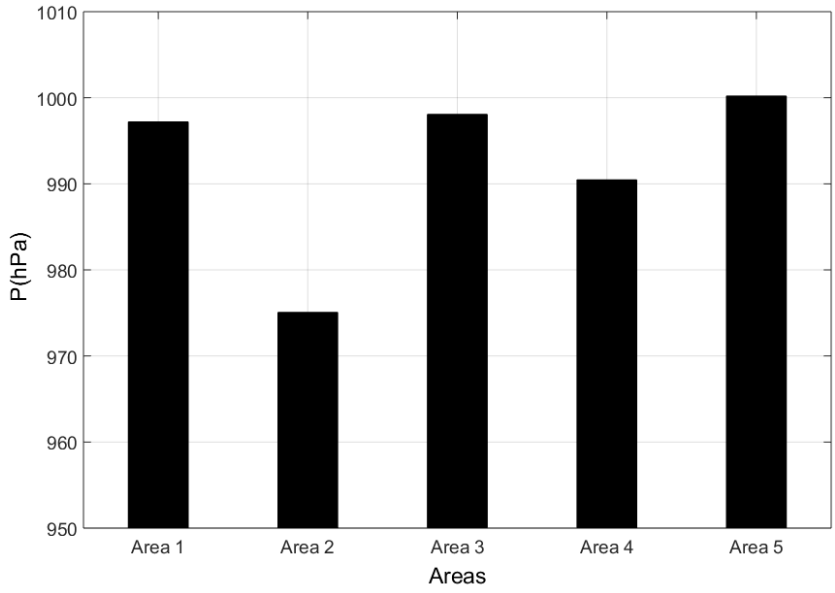

Figure 3: Mean yearly variations of P by area

From Figure 3 we can observe that the yearly mean values of P for area 2 and area 4 are low in comparison for the same values for area 1, area 3, and area 5. For these areas, the mean values of P are very close.

The comparison of reduced to sea level of the obtained mean yearly values (i.e., the values we adopted here) of N_s with the correspondent values of ITU shows that the values are different but similar as shown in Figure 4. This difference is due to the fact in our case more local data has been used to estimate the value of N_s. The reduced to sea level refractivity is used to remove the elevation dependence of the surface refractivity.

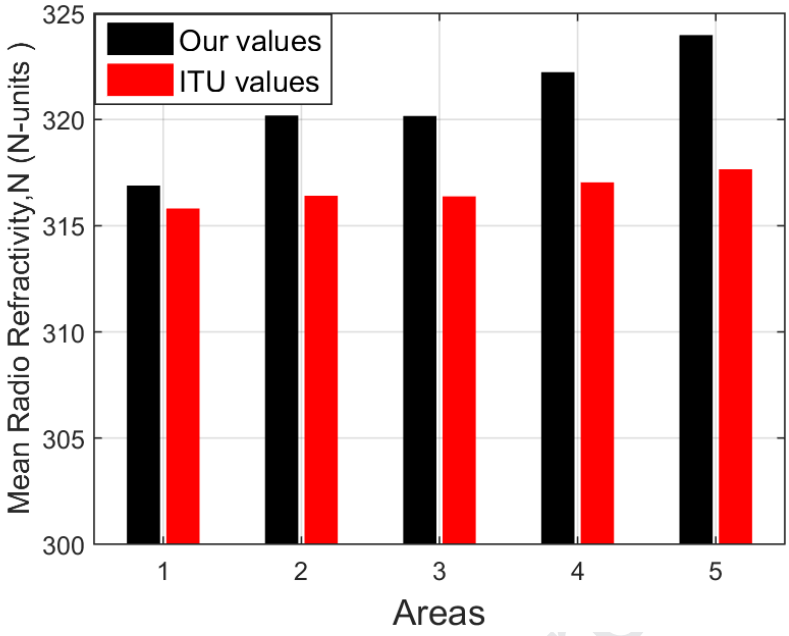

Figure 4: Reduced to sea level mean yearly values of N_s

The results also show that there is a weak dependence of the mean yearly values of water vapour pressure and temperature with the altitude. Figures 5 and 6 show that despite the stations in the identified areas have various altitudes there is a regular increase of e and T from area 1 to area 5. Thus, the mean yearly values of e and T depend more on latitude than the altitude in the analyzed range of the altitude.

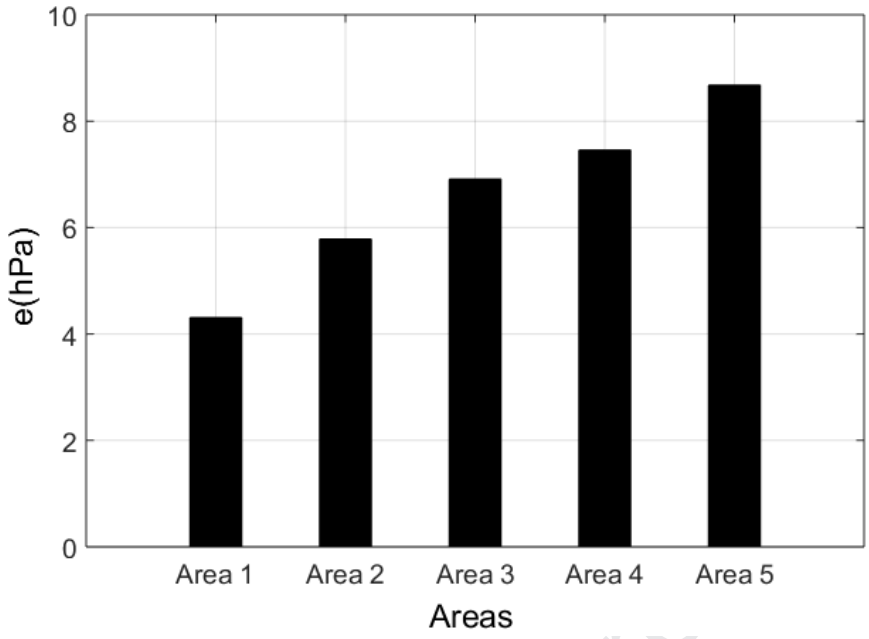

Figure 5: Mean yearly value of e by area

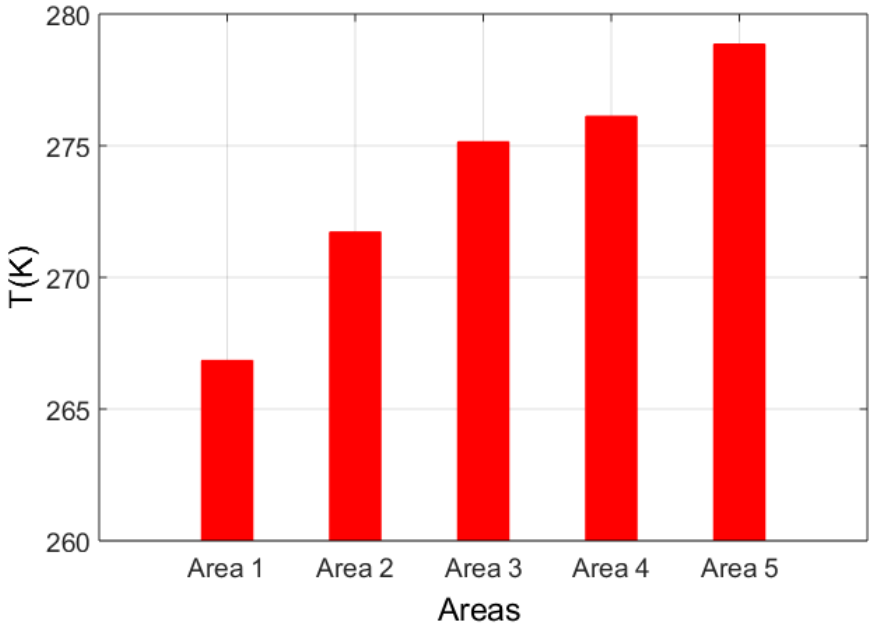

Figure 6: Mean yearly value of T by area

4.3 Analysis of the monthly variations of Ns in various Areas

In this subsection, the monthly variations of *Ns* in various areas will be analysed. In each area the monthly variations of N_s obtained based on data collected from all or some stations as

well as the mean variation of N_s will be represented. The mean monthly variations of N_s estimated based on the data measured from stations located in area 1 are shown in Figure 7.

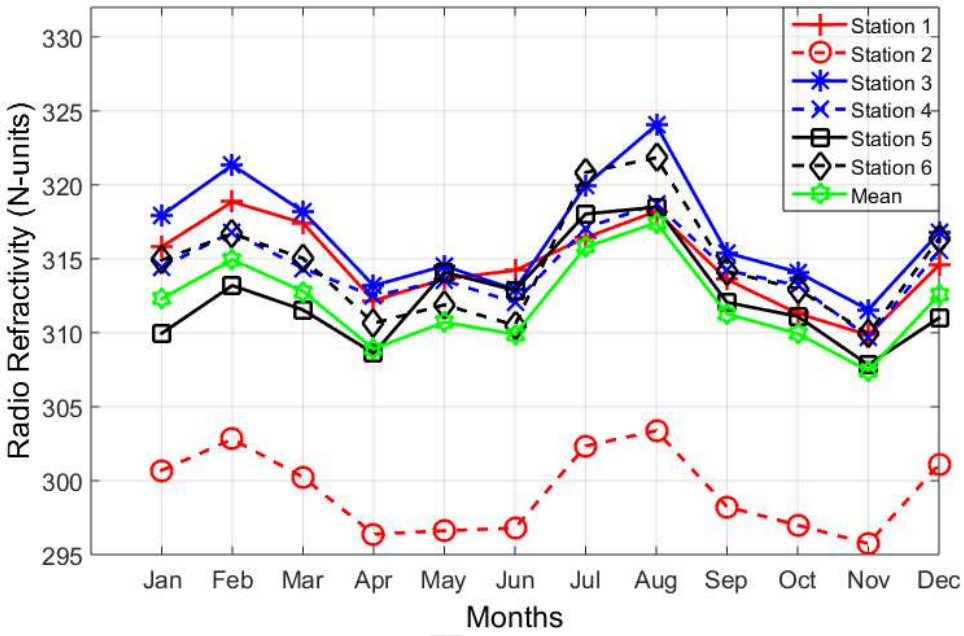

Figure 7: Mean monthly variations of N_s in area 1.

From Figure 7 we can note that seasonal variations of N_s for various stations have different values. This is because the stations have different altitudes (Table 1). Among these stations the values of N_s for the station 2 (Parc Pingualuiyt in Table 1) are particularly low since the altitude of this station is very high (503.4 m) in comparison to the altitudes for the rest stations. However, we can note that all variations of N_s in this area have similar behaviour. In general, the variations have their maximum and the minimum values in August and November respectively.

Figure 8 shows the seasonal variations of N_s for the stations located in area 2, from the figure, it can be observed that the values of N_s (except those corresponding to station 7) are low for most of the months, particularly from January to June in comparison to the values of N_s in area 1. These low values are caused by the fact that almost all stations in area 2, except station 7 have high altitude as seen in Table 1. Similar to observation recorded in area 1, in

general, the variations of N_s for area 2 have their maximum and the minimum values in August and November respectively.

The seasonal variations of N_s for several stations located in area 3 are shown in Figure 9. The big difference in N_s values between station 13 and 23 can be regarded due to the difference in stations' altitude where station 13 latitude is 498 m while station 23 has a low altitude of 5 m. In this area, most of the variations have their maximum values in August and their minimum values in the period from February to April. A similar observation was recorded for areas 4 and 5 where most of the variations have their maximum values in August and their minimum values in March.

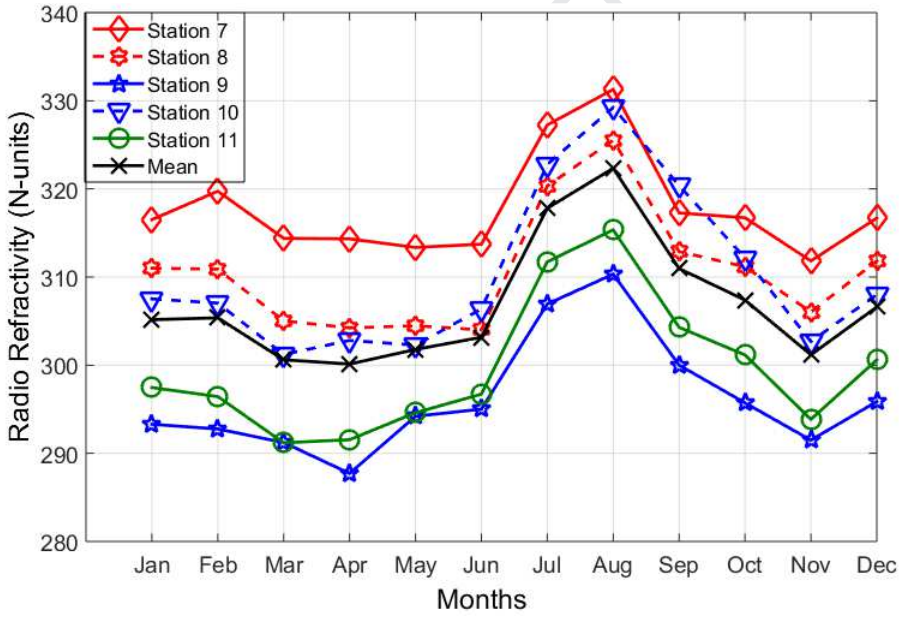

Figure 8: Mean monthly variations of N_s in area 2

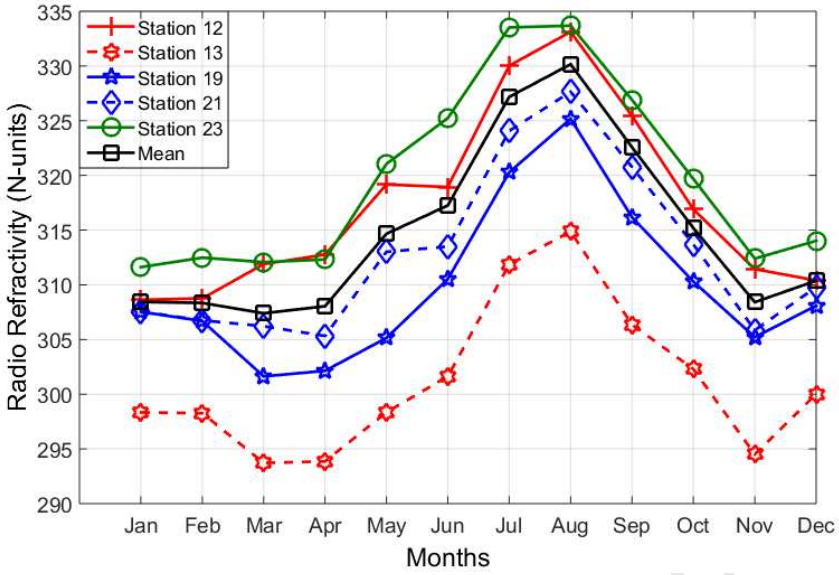

Figure 9: Mean monthly variations of N_s in area 3

5. CONCLUSIONS

A clustering analysis which uses mean monthly variations of water vapour pressure estimated from the data collected in various climatic regions over Quebec has been used to obtain 5 areas from North to South. Despite the presence of mountainous areas, the average yearly value of the *Ns* over Quebec has found to vary in a relatively small interval from 307 N-units to 319 units. This is mainly because the mean yearly variations of *P* have similar values from the North to the South. The water vapour pressure and temperature depend mainly on the latitude. The obtained results show that despite the stations have different altitudes and longitudes the mean yearly values of *e* and *T* increase from North to South.

Independently of the latitude, the altitude of the given region has a significant effect on the value of N_s. The mountainous areas (with high altitude) have shown low values of N_s in comparison with non-mountainous areas. The parameter that mostly contributes to the decrease of N_s is the atmospheric pressure. In the extreme South region (area 5 in this

paper) of Quebec N_s has its maximum value in July. In the remaining areas, the maximum value is observed in August.

References

Aboualmal, A., Abd-Alhameed, R. A., Al-Ansari, K., Alahmad, H., See, C. H., Jones, S. M. & Noras, J. M. 2013. Statistical Analysis of Refractivity Gradient and β_0 Parameter in the Gulf Region. IEEE Transactions on Antennas and Propagation, 61**,** 6250-6254.

Akpootu, D. & Iliyasu, M. 2017. Estimation of tropospheric radio refractivity and its variation with meteorological parameters over Ikeja, Nigeria. Journal of Geography, Environment and Earth Science International**,** 1-12.

Ali, S., Malik, S. A., Alimgeer, K. S., Khan, S. A. & Ali, R. L. 2012. Statistical estimation of tropospheric radio refractivity derived from 10 years meteorological data. Journal of atmospheric and solar-Terrestrial physics, 77**,** 96-103.

Ayantunji, B., Okeke, P., Urama, J. & Najib, Y. 2011. A Semi-Empirical Model for Vertical Extrapolation of Surface Refractivity over Nigeria. The African Review of Physics, 6.

Dubes, R. C. & Jain, A. K. 1988. Algorithms for clustering data. Prentice-Hall Englewood Cliffs.

Freeman, R. L. 2006. Radio system design for telecommunication, John Wiley & Sons.

Guo, G. & Li, S. 2000. Study on the vertical profile of refractive index in the troposphere. International Journal of Infrared and Millimeter Waves, 21**,** 1103-1111.

ITU 2017. ITU-R P.453-13: The radio refractive index: its formula and refractivity data. ITU-R Geneva.

Kablak, N. 2007. Refractive index and atmospheric correction to the distance to the Earth's artificial satellites. Kinematics and Physics of Celestial Bodies, 23**,** 84-88.

Kaufman, L. & Rousseeuw, P. J. 2009. Finding groups in data: an introduction to cluster analysis, John Wiley & Sons.

Kehinde, D. 2018. Analysis of Radio Refractivity Variations Across Geographical Coordinates of Nigeria.

Mathworks, T. 2013. Statistics Toolbox User's Guide The MathWorks. Inc., USA.

Norland, R. Temporal variation of the refractive index in coastal waters. Radar Symposium, 2006. IRS 2006. International, 2006. IEEE, 1-4.

Priestley, J. & Hill, R. 1985. Measuring High–Frequency Refractive Index in the Surface Layer Journal of Atmospheric and Oceanic Technology, Vol. 2.

Recommendation, I. 1999. Reference Standard Atmospheres. ITU-R.

Recommendation, I. 2001. 453-8, The Radio Refractive Index: its formula and Refractivity Data. Recommendations and Reports of the ITU-R.

Serdega, V. & Ivanovs, G. 2007. Refraction seasonal variation and that influence on to GHz range microwaves availability. Elektronika ir Elektrotechnika, 78**,** 39-42.

Sizun, H. & De Fornel, P. 2005. Radio wave propagation for telecommunication applications. Springer.

Zilinskas, M., Tamosiunaite, M., Tamosiuniene, M., Valma, E. & Tamosiunas, S. Gradient of radio refractivity in troposphere. Progress In Electromagnetics Research Symposium Proceedings, Moscow, Russia, August, 2012. 19-23.

- Clustering analysis has been used to identify areas with similar surface refractivity values from North to South. We found that the best input data for the clustering analysis is the water vapour pressure.

- The results show that the surface refractivity increase from North to South. Regardless of the area, the maximum values of the surface refractivity lie in summer.

- In the same area, the mountainous localities have relatively low values of the surface refractivity. This is due mostly to the fact that the atmospheric pressure decreases with the altitude.